Low atmospheric CO_2 during the Little Ice Age due to cooling-induced terrestrial uptake

[NOTE: This is not the published version. For a free Open Access view-only version of the final published version please go to: http://rdcu.be/jrqR]

Rubino, M.[1,*] Etheridge, D.M.[1] Trudinger, C.M.[1] Allison, C.E.[1] Rayner P.J.[2] Enting, I.[1,3] Mulvaney, R.[4] Steele, L.P.[1] Langenfelds, R.L.[1] Sturges, W.T. [5] Curran, M.A.J.[6,7] Smith, A.M.[8]

[1] CSIRO Oceans and Atmosphere, PMB 1, Aspendale, Victoria, 3195, Australia.

[2] School of Earth Sciences, University of Melbourne, 3010, Victoria, Australia

[3] ARC Centre of Excellence for Mathematics and Statistics of Complex Systems (MASCOS), University of Melbourne, 3010, Victoria, Australia

[4] British Antarctic Survey, Madingley Road, Cambridge CB3 0ET, UK

[5] Centre for Ocean and Atmospheric Sciences, School of Environmental Sciences, University of East Anglia, Norwich, Norfolk NR4 7TJ, UK

[6] Australian Antarctic Division, 203 Channel Highway, Kingston Tasmania 7050, Australia

[7] Antarctic Climate and Ecosystems Cooperative Research Centre, University of Tasmania, Hobart 7001, Australia

[8] Australian Nuclear Science and Technology Organisation (ANSTO), PMB 1, Menai, NSW 2234, Australia

* now at: Dipartimento di matematica e fisica, Seconda Università di Napoli, viale Lincoln 5, 81100 Caserta, Italy

Low atmospheric carbon dioxide (CO_2) concentration[1] during the Little Ice Age has been used to derive the global carbon cycle sensitivity to temperature[2]. Recent evidence[3] confirms earlier indications[4] that the low CO_2 was caused by increased terrestrial carbon storage. It remains unknown whether the terrestrial biosphere responded to temperature variations, or there was vegetation re-growth on abandoned farmland[5]. Here we present a global numerical simulation of atmospheric carbonyl sulfide in the pre-industrial period. Carbonyl sulfide concentration is linked to changes in gross primary production[6] and shows a positive anomaly[7] during the Little Ice Age. We show that a decrease in gross primary production and a larger decrease in ecosystem respiration is the most likely explanation for the CO_2 decrease and carbonyl sulfide increase. Therefore, temperature change, not vegetation re-growth, was the main cause for the increased terrestrial carbon storage. We address the inconsistency between ice core CO_2 records from different sites[8] measuring CO_2 and $\delta^{13}CO_2$ in ice from Dronning Maud Land (Antarctica). Our interpretation allows us to derive the temperature sensitivity of pre-industrial CO_2 fluxes for the terrestrial biosphere (γ_L = -10 to -90 PgC K^{-1}), implying a positive climate feedback and providing a benchmark to reduce model uncertainties[9].

Models of future carbon cycle-climate changes predict a large range in atmospheric carbon dioxide (CO_2) concentrations, mainly because of uncertainties in the response of the terrestrial carbon cycle to the future temperature increase[9]. While the carbon cycle is currently dominated by the effect of anthropogenic CO_2 ('fertilization'), pre-industrial records of temperature driven-CO_2

changes provide a way to quantify the size of temperature-carbon cycle feedbacks. The Little Ice Age (LIA, 1500-1750) was a widespread[10] cool period that coincided with low CO_2 concentrations[1] (Figure1a). The CO_2 change made only a minor contribution to the cooling[1], therefore the LIA is a suitable epoch from which to derive the carbon cycle sensitivity to temperature[2].

It has recently been shown that changes in terrestrial organic carbon storage best explain the observed multi-decadal variations in CO_2 concentrations over the past millennium[3]. However, there are open questions about the size of the atmospheric LIA CO_2 decrease[8] and whether it was caused predominantly by the temperature response of land[4], or by land use change following pandemics[5]. To accurately determine the terrestrial carbon cycle's sensitivity to temperature (γ_L) from the LIA records, it is crucial to clearly identify the cause of the LIA CO_2 decrease and to precisely quantify its size.

The net terrestrial CO_2 flux to/from the atmosphere depends on the difference between Net Primary Production (NPP) and Heterotrophic Respiration (R_h). Two hypotheses have been proposed to explain the low CO_2 during the LIA: 1) global NPP increased due to widespread abandonment of farms caused by pandemic diseases[11]; 2) global NPP decreased due to the effect of temperature, but R_h reduced proportionately more due to its higher sensitivity to temperature[4].

Carbonyl sulfide (COS) and CO_2 are both removed from the atmosphere by plants through leaf stomata. Unlike CO_2, however, COS is hydrolysed by the enzyme carbonic anhydrase and there are no major emissions of COS back to the atmosphere from the terrestrial biosphere at the global scale, other than from biomass burning[12]. Carbonyl sulfide has been used to investigate variations of the recent gross terrestrial carbon flux[12], as the atmospheric COS concentration over land varies as a function of Gross Primary Production[6] (NPP=GPP-R_a, Autotrophic Respiration). The record of COS from Siple Dome ice covering the last 350 years, merged with the more smoothed 2000 year

record from SPRESSO ice[7], shows a positive anomaly of COS concentration during the LIA compared to the preindustrial average (Figure 1a). We interpret the positive COS anomaly as an effect of a decrease in GPP at the global scale, assuming that COS emissions from the ocean did not significantly change during the LIA. To test our hypothesis, we quantify the perturbation of the pre-industrial COS budget due to a temperature decrease. We write a COS budget for present times[12] with uncertainties associated with the fluxes[13]. We write the sinks to soil, canopy and chemical removal (mostly driven by hydroxyl radical, OH·) using first-order kinetics with coefficients (k_{soil}, k_{canopy} and k_{OH}) derived from their modern values[12]:

$$F_{oc\text{-}COS} + F_{oc\text{-}DMS} + F_{oc\text{-}CS2} + F_{ant\text{-}COS} + F_{ant\text{-}CS2} + F_{ant\text{-}DMS} + F_{fire\text{-}COS} + F_{oc\text{-}phot\text{-}COS} = [COS] * (k_{OH} + k_{canopy} + k_{soil}) \quad (1)$$

where oc = ocean, ant = anthropogenic, and source terms are from left to right: the direct oceanic COS flux (photochemical); the indirect oceanic fluxes as dimethyl sulfide (DMS) and carbon disulfide (CS_2), both quickly oxidised to COS; the direct anthropogenic COS flux; the indirect anthropogenic fluxes as CS_2 and as DMS; biomass burning; an additional photochemical ocean flux previously used to balance the budget[12]. We then use the same terms and ks to write a pre-industrial COS budget, setting the anthropogenic COS emissions to zero and halving the biomass burning COS source (see Methods and Supplementary Table 1). To simulate the pre-industrial to LIA COS variation, we assume the same relative decrease in GPP and R_h as those given by the Q_{10} factor of the one-dimensional global carbon cycle model[4] for an idealized temperature change of 1 °C (4.8 % for GPP corresponding to the canopy uptake sink, k_{canopy}, and 5.2 % for R_h, associated with the soil sink, k_{soil}). We calculate a pre-industrial to LIA COS increase of 18 ppt, which is in the same direction as (though smaller than) the measured anomaly[7] (Figure 1a). To attribute a likelihood to the COS increase, we set uncertainties of the source terms at 20% of the modern values, assuming that most source processes will change relatively little, and uncertainty in the

turn-over rates at 10% of preindustrial values. With this configuration, the calculated reduction in GPP is significant at the 95% level. In summary, the contemporaneous CO_2 decrease and COS increase can be explained by the reduced temperature during the LIA, causing GPP, NPP and R_h to decrease, with the respiration reduction dominating due to its higher temperature dependence.

Figure 1

Different explanations are unlikely. A decline in farming activity during the LIA would have increased global GPP due to vegetation re-growth, thus decreasing atmospheric COS, and meaning that pandemic-induced abandonment of farms was not the main cause of the atmospheric CO_2 decrease[5,11]. Our finding agrees with modelling results showing that the effect of anthropogenic land use change on atmospheric CO_2 was negligible during the LIA[14], and that there was a net flux of carbon into the European terrestrial biosphere due to increased soil carbon storage as a result of cooling[15]. The net long-term effect of the LIA biomass burning decline[16] on CO_2 is uncertain, due to vegetation re-growth after fire. However, a reduction in biomass burning would have decreased COS. Our interpretation supports the negative γ_L found by CMIP5[17] (Coupled Model Intercomparison Project), that is, a positive climate feedback of terrestrial carbon.

These findings allow us to estimate γ_L from the pre-industrial period. There are numerous regional, continental and global temperature reconstructions available over the last millennium (Figure 1b and c show those[18,19,20,21] used in the following calculation of γ_L). However, there are inconsistencies between different LIA CO_2 records, including the high accumulation rate sites DSS (Law Dome, East Antarctica[1]) and WAIS Divide (West Antarctic Ice Sheet[8]), and the low accumulation rate sites South Pole and EDML (EPICA Dronning Maud Land[22]). The WAIS CO_2 record is 3-6 ppmv higher than the DSS CO_2 record[8], and the cause of the offset remains elusive[8].

To provide further insights into CO_2 variations during the LIA, we have measured the CO_2 concentration in air extracted from the medium resolution Antarctic ice core Dronning Maud Land (DML) covering the period 1300-1900 (Figure 2a). Figure 2b shows the records from DSS[1,23] and WAIS[8].

The gas age distribution of DML (68 % width = 65 years, Figure 2c) is wider than that of DSS (68 % width = 8 years) and WAIS[24] (68 % width = 19 years). Therefore, DML provides a more smoothed record of atmospheric composition changes than DSS and WAIS.

Figure 2b shows the most likely (dotted blue line) atmospheric CO_2 history providing the closest (see SI3.2 for details) reconstruction to the DSS observation once smoothed with the DSS age distribution (solid blue line). The DSS-derived atmospheric CO_2 record smoothed with the DML age distribution closely reproduces the LIA CO_2 decrease measured in DML ice (compare red line and red circles in Figure 2a), providing evidence that the CO_2 records from DSS and DML are compatible (largest difference = 2.1 ppm). On the contrary, the WAIS-derived atmospheric CO_2 history smoothed with the DML age distribution (dashed, red line in Figure 2a) shows higher values than the new DML CO_2 record for all ages, confirming the CO_2 offset in WAIS.

Figure 2

To partition the contribution from the terrestrial biosphere and the oceans to the total CO_2 decrease, we have measured the $\delta^{13}C$ change between 1300 and 1900 in DML ice (Figure 3a). With improved methodology[24], and using ice suitable for CO_2 analyses (with low carbon monoxide levels, SI4.2), we have carried out reliable and high precision $\delta^{13}C$ measurements of CO_2 extracted from ice bubbles (typical total uncertainty for DML: 0.05 ‰). A Kalman Filter Double Deconvolution (KFDD[25]) of the DML $\delta^{13}CO_2$ and CO_2 changes confirms that the terrestrial

biosphere was the main contributor to the atmospheric CO_2 decrease (Figure 3b). The oceans response to the atmospheric change partially counters the terrestrial flux (Figure 3c).

Figure 3

Carbon cycle-climate model simulations of the LIA CO_2 have often combined the data from different ice cores[26], without consideration of the different air age resolution of the cores. We take advantage of the higher resolution information available from DSS to estimate γ_L. It is likely that the LIA CO_2 net flux was mostly driven by the high-latitude Northern Hemisphere terrestrial response to temperature because: 1) the Northern Hemisphere contains most of the world's terrestrial biosphere; 2) the LIA temperature reconstructions showing the best correlation with the CO_2 decrease (Figure 1b) are from the high-northern latitude regions[18,20] and, specifically, the Arctic[3,21]. Therefore, to derive γ_L, we use a number of Northern Hemispheric temperature reconstructions[18,19,20] (Fig 1b) together with the DSS CO_2 record[1,23].

We use a timescale-dependent characterisation[27] of the response of the carbon cycle to estimate the strength of the temperature influence (Methods). This provides a coherent quantification of temperature-to-carbon feedbacks and reconciles previous studies[2,3,26] with consistent use of γ_L and appropriate recognition of time scales. The carbon cycle response is represented by a response function consisting of a sum of exponentials[28]. We parameterise the terrestrial response in terms of γ' (Pg of C yr^{-1} K^{-1}) with a re-adjustment on 100 year timescales. This can be related to γ (Pg of C K^{-1}) with the dependence on τ, the timescale of variation given by $\gamma = -\gamma'/(1/\tau + 1/100)$. Our fits are consistent with fitting timescales of 100 years so that $\gamma \approx -50\,\gamma'$. We obtain γ' for various regions, X, by fitting temperature records T_X to give estimates γ'_X and applying scale factors that characterise the relation between global and regional changes. We derive a range of γ' (see Supplementary Table 2) that corresponds to γ_L in the range: -10 to -90 Pg of C K^{-1} when using a

factor of 2/3[29] to convert NH γ_L to global. This estimate of the temperature sensitivity of terrestrial carbon stores can be used to constrain model predictions of future CO_2 and temperature in CMIP6.

The first model interpretation of the LIA COS increase demonstrates that cooling, rather than recovery from land use, was the main cause of the LIA CO_2 uptake. Our finding argues against the recent suggestion that 1610 could mark the beginning of the Anthropocene[30]. COS concentration shows great potential as an independent measure of pre-industrial CO_2 fluxes that will be improved with additional ice core data and reduced uncertainty in the source terms.

Methods

COS model

We divide the last 700 years into 3 time slices: Present (industrial), Pre-industrial and LIA. The magnitudes of terms (sources and sinks) in equation (1) for the three time slices are reported in Supplementary Table 1. The inverse residence times (rate coefficients) are calculated as the ratio of each sink to the atmospheric COS concentration (k_{OH}= 101/484 = 0.21, k_{canopy}= 738/484 = 1.52, k_{soil} = 355/484 = 0.75) for time slice "Present", which is out of balance by 74.5 Gg of S/year. We write a preindustrial COS budget by setting the anthropogenic COS emissions to zero, halving the biomass burning flux[31] and using the inverse residence times calculated for "Present". With an average preindustrial COS concentration of 330 ppt[7], we derive a budget unbalanced by 132 Gg of S for the pre-industrial period (Table S1), meaning that an atmospheric COS concentration of 383.5 ppt would be required to balance the budget (with corresponding sinks of 80, 585 and 281 Gg of S/year). We associate the uptake of COS by canopy and soil to photosynthesis (GPP) and heterotrophic respiration (R_h), respectively[12,32]:

$k_{canopy} = K_{canopy} * GPP$; $k_{soil} = K_{soil} * R_h$

We simulate the effect of changes in GPP and R_h during the LIA by scaling k_{canopy} and k_{soil} to the same relative changes used by the one-dimensional global carbon cycle model[4] (4.8 % and 5.2 % respectively) for an idealised temperature change of 1 °C (the maximum change for the Northern Hemisphere land, where the effect is most relevant). GPP is often assumed to be roughly twice NPP and it is reasonable to assume a similar Q_{10} value for both. k_{canopy} and k_{soil} become 1.45 [(1.52-

1.45)/1.52*100=4.8%] and 0.70 [(0.73-0.70)/0.70*100=5.2%] respectively. Assuming a balanced budget, we calculate a COS concentration of 401.6 ppt for the LIA, corresponding to a pre-industrial-to-LIA atmospheric COS concentration increase of 18 ppt (401.6-383.5 ppt). Even with uncertainty in the source terms of 30% of modern values, GPP reduction is significant at the 90% level.

We note that autotrophic respiration (R_a) does not have an influence on the COS budget because COS is hydrolysed by plants. We also note that an anoxic soil source may have a strong temperature dependence[33] suggesting that for some times and locations the soil source can overwhelm the soil sink. However, plant uptake generally dominates the COS budget over land. This observation allows us to assume that sources of COS from soils can be considered negligible on the global scale.

The reforestation assumed by the early anthropogenic hypothesis implies a significant shift from C_4 to C_3 productivity. Considering that Leaf Relative Uptake (LRU) is 60 % higher for C_3 than C_4 plants[34] and that COS uptake can be approximated as GPP × LRU × (COS/CO_2) mixing ratio, the C_4 to C_3 shift should have driven a decrease in COS, not the observed increase.

CO_2 uptake responds to changes in CO_2 concentration, the so-called "CO_2 fertilisation effect", which increased CO_2 uptake over the industrial period. This has been hypothesised to contribute to an increase of COS concentration during the Industrial period[31]. A reverse effect of decreased CO_2 on CO_2 uptake probably occurred in the LIA, but it would have either not affected or have led to a small decrease in COS, as lower CO_2 concentration would have opened more stomata and increased COS uptake. For a steady-state solution with fixed sources, the LIA CO_2 decline of 1.5-2% (Fig. 2) and a corresponding GPP decline of 5% would result in a COS rise of 3%. This is assuming

the LRU does not change and the soil sink is more or less in one-to-one correlation with the canopy sink.

To test the sensitivity of the COS result to changes in the photochemical ocean fluxes used previously to balance the budget[12] (this is the main and most uncertain source term), we repeat the calculation described in the main text with a number of different photochemical ocean fluxes. In Supplementary Table 1, the case that would balance the preindustrial budget is shown in parentheses (469 GgS instead of 600 GgS). For this photochemical ocean flux we find a pre-industrial-to-LIA atmospheric COS concentration increase of 16 ppt (330 to 346 ppt, compared to 18 ppt found with a photochemical ocean flux of 600 GgS), suggesting that the simulated pre-industrial-to-LIA COS anomaly does not depend strongly on the magnitude of ocean emissions of COS. If we combine the direct and the additional ocean photochemical fluxes into one term in our analysis, our conclusions would not be affected.

It is worth noting that a number of mechanisms (photochemical and dark production, hydrolysis, air-sea gas exchange, and vertical mixing) contribute to the direct ocean-atmosphere flux of COS[35,36], plus the indirect flux due to the conversion of carbon disulfide (CS2) and dimethylsulfide (DMS) to COS by atmospheric oxidation processes. Based on the complex nature of the relationship between climate and oceanic fluxes, it is unlikely that the processes contributing to the oceanic flux of COS would have all responded to a changing climate in the same direction during the LIA. It is thus difficult to estimate pre-industrial to LIA changes of the net ocean-atmosphere COS flux and use them in our simple approach. Finally, we have also tested the sensitivity of our result to changes in the biomass burning flux[31] and we have not found any significant change (data not shown).

The positive LIA COS anomaly found in the LIA[7] needs to be confirmed in order to constrain more sophisticated CO_2/COS models. A recent study[37] has focused on the last 8000 years and does not have the resolution required to look at the LIA in detail. A new high resolution record of COS is needed for further investigation of the change of atmospheric COS during the LIA.

The relationship between GPP, CO_2 and COS is complicated and our simple model does not address all of the details of it. However, our analysis captures the main elements of the budget and consistently leads to our conclusion that cooling, rather than recovery from land use, was the main cause of the LIA CO_2 uptake.

Antarctic sampling sites

The DML ice core was drilled dry with an electromechanical drill from Dronning Maud Land (77°S, 10°W; 2300m asl, Fig. S1) during the 1997/1998 austral summer[38]. The site has a mean annual temperature of -38 °C and a relatively high snow accumulation rate (70 kg m^{-2} yr^{-1}) compared with the Antarctic plateau, though much lower than Law Dome. Eighteen firn air samples[39] were taken starting from the surface to the firn-ice transition zone at 73.5 m and used to constrain the firn diffusion model[40,41]. The ice age scale for DML has been defined using a combination of layer counting, correction for densification, then a glaciological thinning model guided by several volcanic markers in the non-sea salt sulphate observed in the core and correlated across to other well-dated cores[42].

A second high resolution core, DSS0506 from Law Dome, reaching back only to 1700 AD (gas age), is used to extend the new record from DML to more recent times, link with CO_2 measurements

over the industrial period (SI4.1), and show that the DML records are compatible with the CO_2 and $\delta^{13}C\text{-}CO_2$ reconstructions over the last two centuries[23]. DSS0506 was thermally drilled in a dry hole during the 2005/2006 austral summer in the DSS region of Law Dome (66°46'S, 112°48'E; 1370 m asl, Supplementary Figure 1). The site has high snow accumulation rate (600 kg m^{-2} yr^{-1}) and a mean annual temperature of -22°C. In the following, measurements from DML and DSS0506 are also compared to the results previously published from the DE08 core (Law Dome, 66°43'S, 113°12'E)[1,23]. The ice age scale for DSS0506 was matched through $\delta^{18}O\text{-}H_2O$ measurements to the ice age scale assigned to previously sampled DSS cores[42]. Locations of the sites are shown in Supplementary figure 1.

Extraction of air from ice cores and analysis of CO_2, $\delta^{13}C\text{-}CO_2$

The extraction of air from ice uses a dry grating technique in the Ice Core Extraction Laboratory (ICELAB) at the CSIRO Aspendale (Australia). The extraction procedure has recently been optimised for $\delta^{13}C\text{-}CO_2$ measurements[23]. Briefly, 0.7–1.0 kg of ice was cooled to –80 °C in a chest freezer for at least 24 h prior to extraction. The ice was then sealed in a stainless steel container containing a perforated inner cylinder and the vessel evacuated to less than 10^{-4} Torr for at least 25 min. The ice was grated by mechanically shaking the container for 10 min. This process yielded on average 70 mL of air at STP, estimated by the extraction line volume and pressure. The air was cryogenically collected in a stainless steel tube welded to a Swagelok valve and soldered to a copper base which was cooled to 23–24 K, after removing water at –100 °C. The sample tube (trap) was warmed in a water bath at room temperature for 5 min, before being connected to the

gas chromatographs and split for manual injection and analyses of CO_2, CH_4, N_2O and CO (within 1 h of the extraction) and to a MAT252 IRMS for $\delta^{13}C$ and $\delta^{18}O$ (within 12 h).

Firn modelling

We used the CSIRO firn model[40,41] to date firn air, calculate the age distributions and provide corrections for gravity and diffusion fractionation.

Inputs to the firn model used for DML are mean annual temperature (-38°C), pressure (730mb), accumulation rate (70 kg m^{-2} yr^{-1}), the depth profile of firn density (spline fit to density measurements) and profiles of closed and open porosity versus density (there are no closed porosity measurements for DML, so we use a spline fit based on closed porosity measurements at DE08-2 with a correction for cut bubbles[40,41]). We calibrated effective diffusivity (or, more accurately, inverse tortuosity) versus porosity to give optimum agreement between the modelled and measured concentration of eight trace gases (Supplementary Figure 2).

For DSS0506, there are no measurements of firn air to tune the firn model diffusivity, and no closed porosity measurements. Considering that DSS and DSS0506 are very close to each other (about 300 m), we assume that DSS0506 has the same characteristics as DSS, and use the same model inputs as used for DSS[23].

Gas diffusion in firn causes the air trapped in ice to be younger then the surrounding ice. The gas-age of each sample can be obtained from the ice-age, considering an ice age-gas age difference. For DML, from the drilling and firn sampling records, the close-off depth, the depth at which it is no longer possible to withdraw air out of the firn with a vacuum pump, is around 72 m. The age of

DML ice at 72 m is 664 years from the drilling date of January 1998, so the year 1334. From our firn modelling, the mean age of CO_2 in air at close-off is 76 years, giving an age difference between ice and air of 588 years for CO_2, which we apply to all samples.

For DSS0506, the ice-air age difference for CO_2 used for DSS is used here (61 years). This number is consistent with previous work[1,23] and provides the age for which measurements of CH_4 concentration in DSS ice best overlap the measured CH_4 at DE08 and DE08-2 ice, and the age which is most consistent with the measured $\Delta^{14}C$-CO_2 bomb pulse[44].

Double Deconvolution

A double deconvolution calculation uses CO_2 and $\delta^{13}C$ to estimate the net fluxes of CO_2 between the atmosphere and terrestrial biosphere and the atmosphere and oceans. We use the new DML CO_2 and $\delta^{13}C$ records in the Kalman Filter Double Deconvolution[25] (KFDD). This combines the statistical analysis of the Kalman Filter, which allows estimation of uncertainties in the fluxes, with CO_2 and $\delta^{13}C$ mass balance from a (globally aggregated) carbon cycle model (needed to calculate the isotopic disequilibrium fluxes). The carbon cycle model we use consists of a two-box terrestrial model and a mixed layer pulse response function of a box diffusion model of the ocean. The KFDD is well suited to interpretation of ice core data with long gaps because it does not assume values for either CO_2 or $\delta^{13}C$ in the data gaps.

Discrepancy between the $\delta^{13}C$ records at DML/DSS and at WAIS.

The difference between the $\delta^{13}C$ records at DML/DSS and at WAIS (Figure 3a) could be due to differences in the calibration scales used at CSIRO and at Oregon State University, or to the effect of *in-situ* production of CO_2 on its $\delta^{13}C$. An inter-comparison between CSIRO and Oregon State University[8] has checked the calibration issue for CO_2, but this has not been done for $\delta^{13}C$ (this is planned), so the reason for the difference is currently unknown. However, the CSIRO records link ice and firn data to well calibrated atmospheric data[23], demonstrating their reliability.

Carbon cycle sensitivity to climate change

Our analysis of temperature sensitivity is based on representing the change in atmospheric carbon mass as:

$$Q(t_j) = \Delta M(t) \sim \int^{t} R(t-t') \int^{t'} H(t'-t'') \, \Delta T(t'') dt' dt'' \qquad \text{(SE1)}$$

i.e. temperature influences carbon fluxes (characterised by response function $H(.)$) and then the carbon cycle (characterised by response function $R(.)$) responds to concentration changes. This is the same conceptual form as[27]:

$$\Delta M = -\left[\frac{1}{1+\beta_O+\beta_L}\right][\gamma_O + \gamma_L]\Delta T \qquad \text{(SE2)}$$

where γ_O and γ_L characterise responses to temperature change and β_O and β_L characterise responses to consequent atmospheric change. The mapping between (SE1) and (SE2) involves 3 steps:

- using the Laplace transform[45] of (SE1);

- recognising the $\frac{1}{1+\beta_O+\beta_L}$ factor as the CO_2 airborne fraction;

- using the general timescale-dependent form of the airborne fraction in terms of Laplace transforms[46].

Thus the Laplace transform generalises (SE2) to include a dependence on the timescale[47] p^{-1} expressing the response to a temperature perturbation, $W(t)$, as:

$$q(p) = -\left[\frac{1}{1+\beta_O(p)+\beta_L(p)}\right][\gamma_O(p) + \gamma_L(p)]w(p) \qquad \text{(SE3)}$$

with lower case symbols used for Laplace transforms[45,46] and $\gamma_O(p) + \gamma_L(p) = -\frac{h(p)}{p}$.

The approach of Bauska[3] differs from our approach by taking the atmospheric response to the left side of equation (1) as a deconvolution (or in practice double deconvolution) operation. Our representation of $H(t)$ is essentially the same as Bauska's one-box model[48]. We parameterise it as

$$h(p) = \gamma' \frac{p}{p+\frac{1}{\tau}} \qquad \text{(SE4)}$$

whence $\gamma(p) = -\frac{\gamma'}{p+\frac{1}{\tau}}$. For the present we take τ = 100 years. The parameterisation used by Bauska[48] seems (assuming that C refers to perturbations) to correspond to

$$h(p) = -\frac{\gamma_B}{\tau}\frac{p}{p+\frac{1}{\tau}} \qquad \text{(SE5)}$$

whence

$$\gamma = \frac{\gamma_B}{\tau\left(p+\frac{1}{\tau}\right)} \qquad \text{(SE6)}$$

Thus although Bauska uses γ to denote the quantity we call γ_B it only corresponds to the definition[27] of γ in the $p \to 0$ limit. Further analysis (to be presented elsewhere) suggests that the β_k estimated for the northern hemisphere[48] correspond to

$$\beta_k = -\gamma' \frac{p\left(p+\frac{1}{\tau_k}\right)}{p+\frac{1}{\tau}} \qquad \text{(SE7)}$$

where the τ_k are the timescales of the exponential smoothing used in the estimation. The various values given by Bauska[3] are consistent with $\gamma \approx$ -46 PgC/K at p^{-1}= 125 years, assuming our preferred values of τ= 100 years.

To construct our own estimates of the sensitivity, we extract γ' as a factor, with $H(.) = \gamma' \widetilde{H}(.)$. We use the associative property of convolutions to write (SE1) as

$$Q(t) = \Delta M(t) \sim \gamma' \int^t \widetilde{R}^*(t-t')\Delta T(t')dt' \qquad \text{(SE8)}$$

where $\widetilde{R}^*$ is the convolution of $R(.)$ and $H(.)$. We express $R(.)$ as a sum of exponentials[28] and $\widetilde{H}(.)$ from the one-box model, so that $\widetilde{R}^*$ is readily expressed as a sum of exponentials.

To account for our use of regional reconstructions of temperature we put:

$$Q(t) = \Delta M(t) \sim \gamma'_X \int^t \widetilde{R}^*(t-t')\Delta T_X(t')dt' \qquad \text{(SE9)}$$

where we introduce factors a_X to relate region X to global temperatures by $\Delta T_X \approx a_X T_{global}$ whence $\gamma' = a_X \gamma'_X$. To provide global estimates we use[29] $a_{NH} = 1.5$ and apply this for both the whole of the northern hemisphere and parts thereof.

The regressions were performed using the "lm" procedure in the programming language R, after calculating $\int^t \widetilde{R}^*(t-t')\Delta T(t')dt'$ at annual time steps. The offset used in defining ΔT affects the intercept of the regression, but not the estimate of γ'.

As explained in the main text, the γ' values shown in Supplementary Table 2 can be converted to γ values simply multiplying them by -50 because our fits are consistent with fitting timescales of 100 years ($\gamma \approx -50\,\gamma'$). Only the temperature reconstructions of the Northern Hemisphere[18,19,20] have been used to derive γ values because we don't attempt a partitioning of the temperature signal into the continental[21] contribution (disaggregation). Having shown that DSS and DML agree well (over the time period of DML measurements: 1300-1900), we now use the entire DSS record over the last millennium (pre-industrial) to derive the terrestrial CO_2 sensitivity to temperature. In Supplementary Table 2, the CO_2 sensitivity to temperature increases (that is, the range of γ values) becomes more negative going from the 500-1750 to the 1500-1800 time period. This is an effect of the increasing weight of the 1610 CO_2 decrease on the total period. Since the 1610 event has not yet been clearly confirmed as a real atmospheric event, we exclude the 1500-1800 period (shown in Supplementary Table 2) from our calculation, because this is the period for which the 1610 event has the highest weight. For the remaining periods, γ is in the range: -11 to -33 PgC K^{-1} (500-1750), -15 to -48 PgC K^{-1} (1000-1750) and -31 to -87 PgC K^{-1} (1300-1750). As we do not find any reason to favour one of the time periods used, the range of γ values is approximated as -10 to -90 PgC K^{-1}. The final estimate of γ is attributed only to land (γ_L) based on the finding from the double deconvolution that the ocean was not responsible for the CO_2 change.

Data availability

The authors declare that the data supporting the findings of this study are available within the article and its supplementary information files.

Code availability

The code used to generate the carbonyl sulfide global numerical model can be accessed on-line.

References

1. MacFarlingMeure, C. et al. Law Dome CO_2, CH_4 and N_2O ice core records extended to 2000 years BP. *Geophys. Res. Lett.* **33,** L14810 (2006).

2. Cox, P. & Jones, C. Climate change — Illuminating the modern dance of climate and CO_2. *Science* **321,** 1642–1644 (2008).

3. Bauska, T. K. et al. Links between atmospheric carbon dioxide, the land carbon reservoir and climate over the past millennium. *Nat. Geosci.* **8,** 383-387 (2015).

4. Trudinger, C.T. Enting, I. G. Francey, R. J. Etheridge, D. M. & Rayner, P. J. Long-term variability in the global carbon cycle inferred from a high-precision CO_2 and $\delta^{13}C$ ice-core record. *Tellus* **51B,** 233-248 (1999)

5. Kaplan, J.O. Climate or humans? *Nat. Geosci.* **8,** 335-336 (2015)

6. Montzka, S.A. et al. On the global distribution, seasonality, and budget of atmospheric carbonyl sulfide (COS) and some similarities to CO_2. *J. Geophys. Res.* **112,** D09302 (2007)

7. Aydin, M. Williams, M. B. Tatum, C. and Saltzman, E. S. Carbonyl sulfide in air extracted from a South Pole ice core: A 2000 year record. *Atmos. Chem. Phys.* **8,** 7533-7542 (2008)

8. Ahn, J. et al. Atmospheric CO_2 over the last 1000 years: A high-resolution record from the West Antarctic Ice Sheet (WAIS) Divide ice core. *Glob. Biogeochem. Cycles* **26,** GB2027 (2012)

9. Friedlingstein P. et al. Uncertainties in CMIP5 Climate Projections due to Carbon Cycle Feedbacks. *J. Clim.* **27,** 511-526 (2014)

10. Neukom R. et al. Inter-hemispheric temperature variability over the past millennium. *Nat. Clim. Chang.* **4,** 362-367 (2014)

11. Ruddiman W.F. The early anthropogenic hypothesis: challenges and responses. *Rev. Geophys.* **45,** RG4001 (2007)

12. Berry J. et al. A coupled model of the global cycles of carbonyl sulfide and CO_2: A possible new window on the carbon cycle. *J. Geophys. Res.-Biogeosci.* **118,** 842-852 (2013)

13. Kettle A.J. Kuhn, U. von Hobe, M. Kesselmeier, J. & Andreae, M. O. Global budget of atmospheric carbonyl sulfide: Temporal and spatial variations of the dominant sources and sinks. *J. Geophys. Res.* **107,** 4658 (2002)

14. Pongratz, J. Caldeira, K. Reick, C. H. & Claussen, M. Coupled climate–carbon simulations indicate minor global effects of wars and epidemics on atmospheric CO_2 between 800 and 1850. *Holocene* **21,** 843-851 (2011)

15. Kaplan, J.O. Krumhardt, K. M. & Zimmermann, N. E. The effects of land use and climate change on the carbon cycle of Europe over the past 500 years. *Glob. Chang. Biol.* **18,** 902–914 (2012)

16. Rubino M., D'Onofrio, A. Seki, O. Bandle, J. Ice-core records of biomass burning. *The Anthropocene Reviews*, DOI: 10.1177/2053019615605117 (2015)

17. Arora, V.K. et al. Carbon–Concentration and Carbon–Climate Feedbacks in CMIP5 Earth System Models. *J. Clim.* **26,** 5289-5314 (2013)

18. Moberg, A. Sonechkin, D. M. Holmgren, K. Datsenko, N. M. & Karlén, W. Highly variable Northern Hemisphere temperatures reconstructed from low- and high-resolution proxy data. *Nature* **433,** 613-617 (2005)

19. Mann, M.E. et al. Global Signatures and Dynamical Origins of the Little Ice Age and Medieval Climate Anomaly. *Science* **326,** 1256 (2009)

20 Christiansen, B. & Ljungqvist F.C. The extra-tropical Northern Hemisphere temperature in the last two millennia: reconstructions of low-frequency variability. *Clim. Past* **8,** 765-786 (2012)

21. PAGES 2k network. Continental-scale temperature variability during the past two millennia. *Nat. Geosci.* **6,** 339-346 (2013)

22. Siegenthaler, U. et al. Supporting evidence from the EPICA Dronning Maud Land ice core for atmospheric CO_2 changes during the past millennium. *Tellus* **57B,** 51-57 (2005)

23. Rubino, M. et al. A revised 1000 year atmospheric $\delta^{13}C$-CO_2 record from Law Dome and South Pole, Antarctica. *J. Geophys. Res-Atmos.* **118,** 8482-8499 (2013)

24. Mitchell, L.E. et al. Observing and modeling the influence of layering on bubble trapping in polar firn. *J. Geophys. Res-Atmos.* **120,** 2558-2574 (2015)

25. Trudinger, C.M. Enting, I. G. Rayner, P. J. & Francey, R. J. Kalman filter analysis of ice core data 2. Double deconvolution of CO_2 and $\delta^{13}C$ measurements. *J. Geophys. Res.* **107,** 4423 2002

26. Frank, D.C. et al. Ensemble reconstruction constraints on the global carbon cycle sensitivity to climate. *Nature* **463,** 527-530 (2010)

27. Friedlingstein, P. Dufresne, J. L. Cox, P. M. & Rayner, P. How positive is the feedback between climate change and the carbon cycle? *Tellus* **55B,** 692-700 (2003)

28. Joos, F. et al. Carbon dioxide and climate impulse response functions for the computation of greenhouse gas metrics: a multi-model analysis. *Atmos. Chem. Phys.* **13,** 2793-2825 (2013)

29. Scheffer, M. Brovkin, V. & Cox, P. Positive feedback between global warming and atmospheric CO_2 concentration inferred from past climate change. *Geophys. Res. Lett.* **33**, L10702 (2006)

30. Lewis, S.L. & Maslin, M.A. Defining the Anthropocene. *Nature* **519,** 171-180 (2015)

31. Campbell, J.E. et al. Atmospheric carbonyl sulfide sources from anthropogenic activity: Implications for carbon cycle constraints. *Geophys. Res. Lett.* **42**, 8: 3004-3010 (2015)

32. Campbell et al. Photosynthetic control of atmospheric carbonyl sulfide during the growing Season. *Science*. **322**: 1085-1088 (2008)

33. Maseyk et al. Sources and sinks of carbonyl sulfide in an agricultural field in the Southern Great Plain. *PNAS*, **111**: 9064-9069 (2014)

34. Stimler, K. Berry, J.A. Montzka, S.A. Yakir, D. Association between COS uptake and $^{18}\Delta$ during gas exchange in C_3 and C_4 leaves. *Plant Physiol.* **157**, 1, 509-517 (2011)

35. von Hobe, M. Najjar, R. G. Kettle, A. J. & Andreae, M. O. Photochemical and physical modeling of carbonyl sulfide in the ocean. *J. Geophys. Res.* **108**, 3229 (2003)

36. Lanois, T. Belviso, S. Bopp, L. Fichot, C. G. & Peylin, P. A new model for the global biogeochemical cycle of carbonyl sulfide - Part 1: Assessment of direct marine emissions with an oceanic general circulation and biogeochemistry model. *Atmos. Chem. Phys. Discuss.* **14**, 20677-20720 (2014)

37. Aydin, M. et al. Carbonyl sulfide hydrolysis in Antarctic ice cores and an atmospheric history for the last 8000 years. *J. Geophys. Res-Atm.* **119**, 8500–8514 (2014)

38. Mulvaney, R. Bremner, S. Tait A. and Audley N. A medium depth ice core drill. *Mem. Natl. Inst. Polar Res.* **56**, Special Issue, 82–90 (2002)

39. Bräunlich, M. et al. Changes in the global atmospheric methane budget over the last decades inferred from ^{13}C and D isotopic analysis of Antarctic firn air. *J. Geophys. Res.* **106**, 20456-20481 (2001)

40. Trudinger, C.M. et al. Modeling air movement and bubble trapping in firn. *J. Geophys. Res.* **102**, 6747-6763 (1997)

41. Trudinger, C.M. et al. How well do different tracers constrain the firn diffusivity profile? *Atmos. Chem. Phys.* **13**, 1485-1510 (2013)

42. Hofstede, M.C. et al. Firn accumulation records for the past 1000 years on the basis of dielectric profiling of six cores from Dronning Maud Land, Antarctica. *J. Glaciol.* **169**, 279-291 (2004)

43. Plummer, C.T. et al., An independently dated 2000-yr volcanic record from Law Dome, East Antarctica, including a new perspective on the dating of the 1450s CE eruption of Kuwae, Vanuatu. *Clim. Past.* **8**, 1929-1940 (2012)

44. Smith, A. et al., In search of in situ radiocarbon in Law Dome ice and firn. *Nucl. Instrum. Meth. B.* **172**, 610-622 (2000)

45. Enting, I.G. Inverse Problems and Complexity in Earth System Science. In: Complex Physical, Biophysical and Econophysical Systems. Proceedings of the 22nd Canberra International Physics Summer School, The Australian National University, Canberra, 8-19 December 2008 (2010)

46. Enting, I.G. Laplace transform analysis of the carbon cycle. *Environ Modell Softw.* **22**, 1488-1497 (2007)

47. Lehner, F. et al. Climate and carbon cycle dynamics in a CESM simulation from 850 to 2100 CE. *Earth Syst. Dyn.* **6,** 411-434 (2015)

48. Bauska, T.K. et al. Carbon Cycle Variability during the Last Millennium and Last Deglaciation. PhD thesis (2013)

Corresponding author: Mauro Rubino, mauro.rubino@unina2.it

Acknowledgments

This work was undertaken as part of the Australian Climate Change Science Program, funded by the Australian government - Department of the Environment, the Bureau of Meteorology and CSIRO. We thank Scott Coram, Rebecca Gregory, David Thornton and Darren Spencer of CSIRO for their analytical support and Sam Allin for ice handling. William Sturges recognises the CSIRO Fröhlich Fellowship for supporting a visit to CSIRO, Aspendale. Mauro Rubino's visit to CSIRO and David Etheridge's visit to the Second University of Naples were supported by Italian POLIGRID project (CUP B65B0900002007). The DML ice was sampled using funding from the Natural Environment Research Council (grant NE/F021194/1). We thank the British Antarctic Survey for providing DML ice samples. The Australian Antarctic Science Program and ANSTO supported drilling of DSS0506 through the AINSE grant and AAS grants 4061 and 3064. We thank Paul Fraser and three anonymous reviewers for their useful comments.

Author contributions

DME conceived the study. DME and MR planned the project. DME, AMS, MAJC, RM, and WTS sampled, dated and provided ice cores. MR, DME, CEA, RLL, and LPS carried out the measurements. CMT developed and run the firn modelling and the KFDD. PJR, MR, CMT and DME

developed the COS model and interpreted the results. IE, MR, DME and CMT performed the carbon sensitivity to temperature analysis. All authors contributed to results interpretation and manuscript writing.

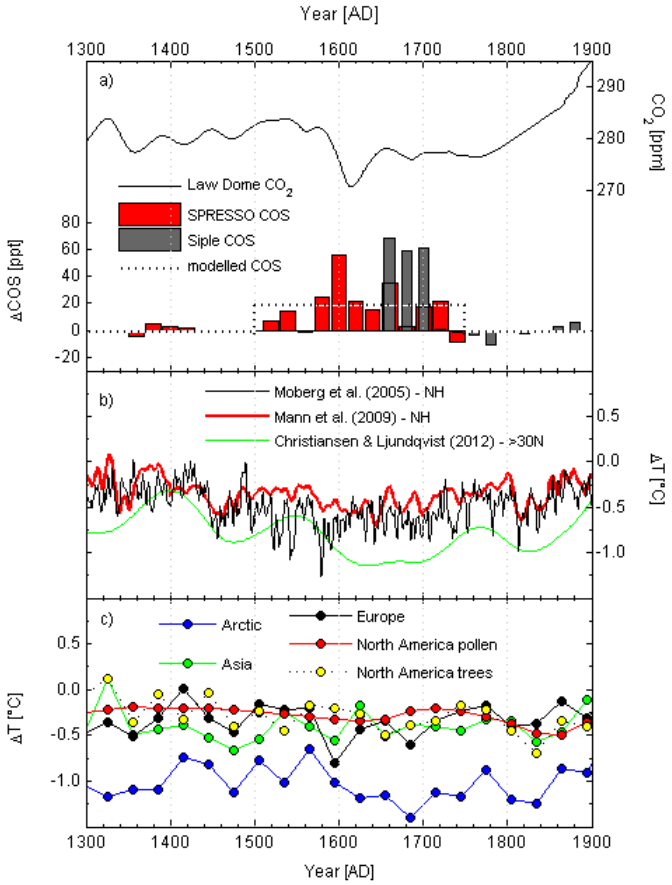

Figure 1| Carbon Cycle and temperature variability over the LIA: Reconstructions of a) atmospheric CO_2 (spline fit to Law Dome[1], solid line) and COS anomaly (20 year aggregated data[7] from the pre-industrial mean of 330 ppt) - the dotted line shows our modelled pre-industrial-to-LIA COS anomaly; b) Northern Hemisphere annual mean (black line is M2005[18] and red line is Mann99[19]) and 50 year-smoothed (green line is CL2012[20]) temperature reconstructions; c) 30 year mean-Northern Hemispheric continental temperature reconstructions from the PAGES2k Network[21]. All temperature reconstructions are expressed as anomalies from the 1961-1990 reference period.

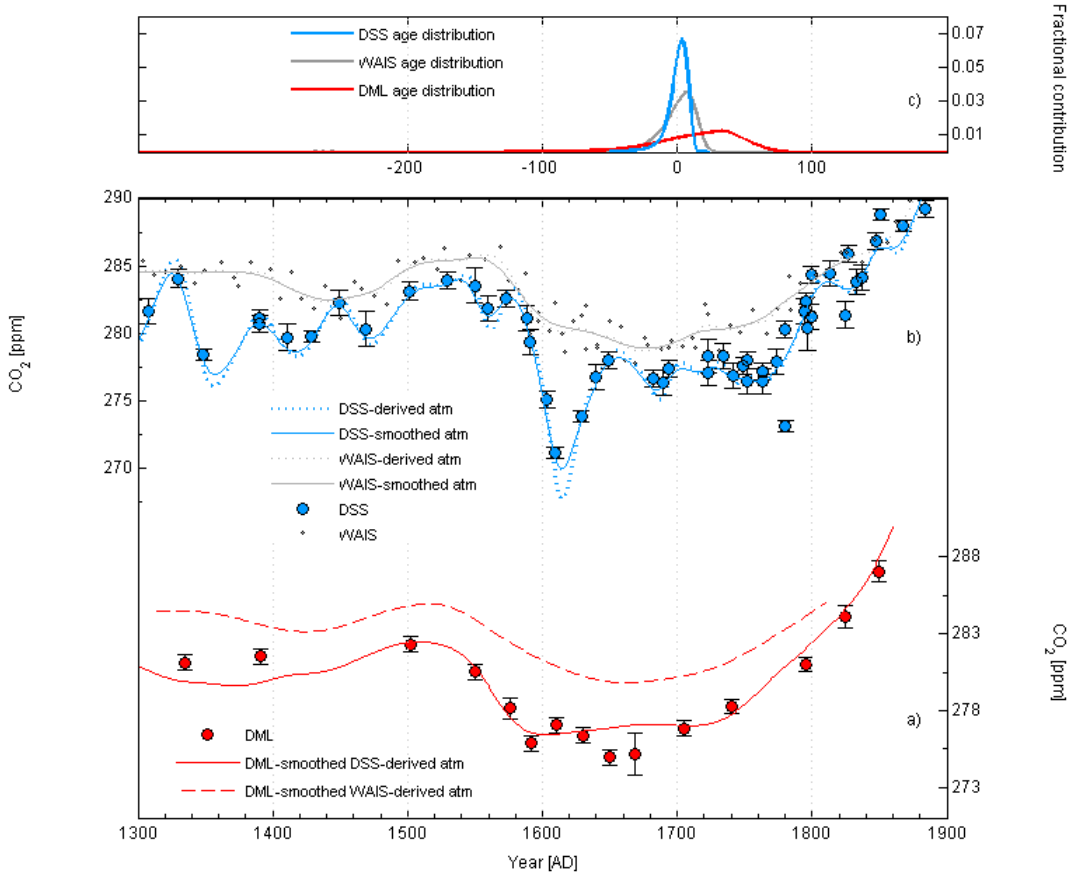

Figure 2| Comparison of CO_2 records: a) DML CO_2 measurements; DSS-derived and WAIS-derived atmospheric reconstructions smoothed with DML age distribution. b) DSS and WAIS CO_2 measurements; DSS-derived and WAIS-derived atmospheric CO_2 reconstruction; DSS-derived and WAIS-derived atmospheric CO_2 reconstruction smoothed with DSS and WAIS age distribution respectively; c) CO_2 age distribution for DML, WAIS and DSS. Error bars are 1σ uncertainties: they are typically 0.6 ppm (range 0.4-1.4 ppm)[23] for DSS and DML CO_2 measurements, whereas they are not reported here for WAIS CO_2 measurements, but are typically 0.8 ppm (range 0.1-2 ppm)[8].

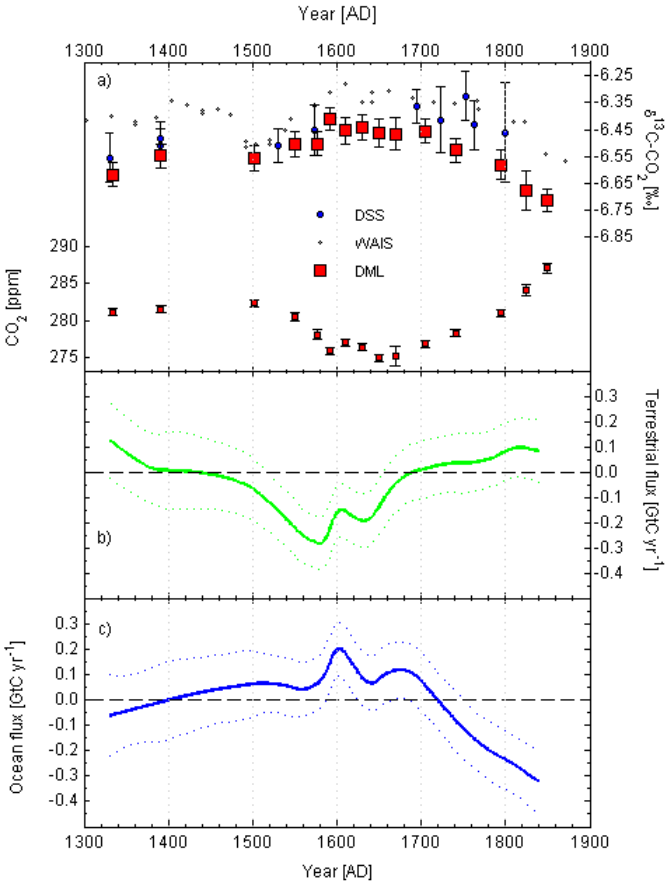

Figure 3| Double Deconvolution of DML CO_2 and $\delta^{13}C$: The new records for a) CO_2 concentration and $\delta^{13}C$ from DML, together with the existing $\delta^{13}C$ measurements from DSS[23] and WAIS[3]. Error bars are analytical uncertainties (typically 0.6 ppm and 0.05 ‰ for DML and 0.1 ‰ for DSS[23]). Error bars for WAIS have not been reported, but are typically around 0.04 ‰[3]. The solid green and blue lines represent CO_2 fluxes and their 1σ uncertainties for b) the terrestrial biosphere-atmosphere and (c) the ocean-atmosphere, calculated in the KFDD[25] using only DML observations.